Modulation of ionic conduction using polarizable surfaces

A. P. dos Santos [1,2] F. Jiménez-Ángeles [2] A. Ehlen [3] and M. Olvera de la Cruz [2,3,4]

[1]*Instituto de Física, Universidade Federal do Rio Grande do Sul, Caixa Postal 15051, CEP 91501-970, Porto Alegre, RS, Brazil*

[2]*Department of Materials Science and Engineering, Northwestern University, Evanston, Illinois 60208, USA*

[3]*Applied Physics Program, Northwestern University, Evanston, Illinois 60208, USA*

[4]*Department of Physics and Astronomy, Northwestern University, Evanston, Illinois 60208, USA*

(Received 16 June 2023; accepted 17 October 2023; published 27 November 2023)

Hybrid ionic-electronic conductors have the potential to generate memory effects and neuronal behavior. The functionality of these mixed materials depends on ion motion through thin polarizable channels. Here, we explore different polarization models to show that the current and conductivity of electrolytes is higher when confined by conductors than by dielectrics. We find nonlinear currents in both dielectrics and conductors, and we recover the known linear (Ohmic) result only in the two-dimensional limit between conductors. We show that the polarization charge location impacts electrolyte structure and transport properties. This work suggests a mechanism to induce memristor hysteresis loops using conductor-dielectric switchable materials.

DOI: 10.1103/PhysRevResearch.5.043174

I. INTRODUCTION

Switchable conductance is desirable for designing densely interconnected (neuromorphic) systems for information storage, performing complex logic operations, and executing neural network algorithms [1–3]. To emulate neural activity, such as voltage spiking [4,5] and synaptic plasticity [6,7], researchers use different materials considering switchable ionic or electronic conduction [8,9]. For example, the gate resistance tunability has been explored for neuromorphic circuits using monolayer MoS_2 multiterminal memtransistors [9]. To expand functionality and flexibility of device design, integration of ionic and electronic conduction is an attractive option, as it may allow for imitating synaptic potentiation, emulating plasticity [10,11], and achieving neural interfacing. The coupling between ionic and electronic transport is promising for leveraging other applications such as biosensing, energy storage, and responsive materials.

Mixed ionic-electronic conductors are materials that conduct both ions and electronic charge carriers (electrons and/or holes) [12]. Recent developments combine electronic and ionic conductor materials into alternating layers of nanometric dimensions where the ionic and electronic conduction occur simultaneously [13]. The close proximity of ionic and electronic charge carriers in these devices means that the conduction behavior of one influences the other. These materials' electronic properties can be modified by the stoichiometry [14,15], gate biasing [9,16], and structural changes [13]. The coupled ionic and electronic interactions and transport need special understanding beyond the comprehension of their independent behavior.

Despite numerous technological applications envisioned by using mixed ionic-electronic conduction, the lack of fundamental understanding impedes rational materials design. One essential component of mixed conduction is the effect of induced electronic polarization on ionic conduction. Previous work showed that the electronic properties of surfaces affect the nearby ions, specifically via the induced polarization charges due to dielectric mismatch on the material-electrolyte interface [17–20]. A recent formalism employs the Thomas-Fermi model [21] to consider polarization effects on the ions' transport in strong confinement by dielectrics and conductors [19]. However, the formalism is derived only for ions constrained to move in two dimensions. Using two different approaches, here we study ion conduction in strong confinement in a slitlike channel and we recover some aspects of the two-dimensional behavior predicted by the Thomas-Fermi model.

Frameworks and models that integrate the interfacial electronic polarization of materials and electrostatic molecular interactions are essential for exploiting the properties of interfaces in nanometer slit confinement [18,20,22]. As illustrated in Fig. 1(a), the electrostatic potential generated by a charge in the center of a narrow, slitlike channel is highly dependent on the polarizability of the channel. Whereas the range of the potential is increased by dielectric confinement, the potential in strong conducting confinement is so screened that it can be considered short range. Here, we study ionic conduction in strongly confining slitlike channels and show that the ionic conductivity and the ionic adsorption are significantly impacted by changes in the confining material polarization (from dielectric and conductor), the confining distance, and the location of the polarization charges. Results from density-functional theory show that the polarization plane location is a material-dependent property [23]. Hence, by adjusting the

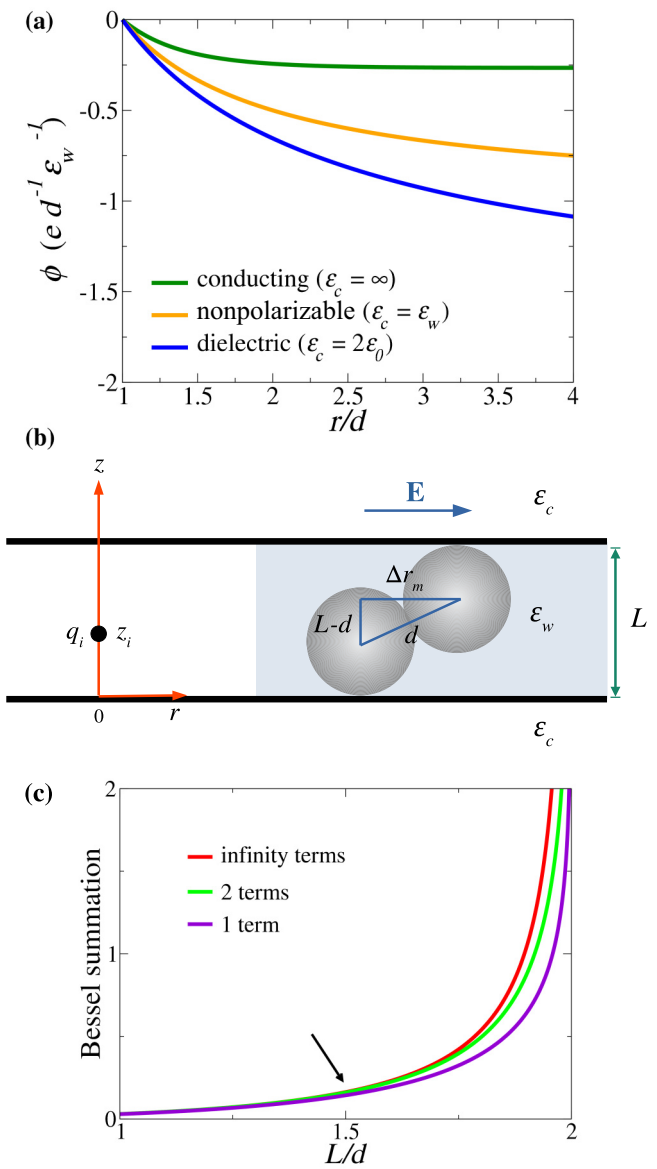

FIG. 1. Ions strongly confined by polarizable surfaces. (a) Electrostatic potential in the radial direction (r) for $\varepsilon_w = 5\varepsilon_0$, from an ion at the center ($z = L/2$, where $L = 1.475d$) of two conducting, nonpolarizable, or dielectric surfaces. We use a $1/r$ potential for nonpolarizable confinement and the traditional method of images for the dielectric and conducting confinements. To aid visualization, the potential is set to zero at $r/d = 1$. (b) The cylindrical coordinate system used to derive the FSCC model and the setup employed in molecular simulations; z and r are the axial and radial coordinates, respectively, and Δr_m is the minimal ion-ion radial separation; **E** is the external electric field applied to investigate the ions' transport in the direction parallel to the surfaces. (c) Convergence of the Bessel summation $\sum_{n=1}^{\infty} K_0(\frac{n\pi \Delta r_m}{L})$ in Eq. (1) for various interplane distances L at the minimum ion-ion separation $\Delta r_m = \sqrt{L(2d - L)}$. The black arrow indicates the largest value of L/d for which we consider the Bessel summation to converge using only the first term.

polarization plane location we consider materials of different electronic properties.

The paper is organized as follows. First, we develop an efficient method for treating ionic interactions in strong confinement by conductors and define the system parameters. We then find a nonlinear ionic conduction response, which is a prerequisite for neuromorphic behavior. Finally, we demonstrate that the location of the polarization charge impacts the ionic distribution and transport through the channel. The placement of the polarization charge offers a mechanism for modeling material-dependent properties of polarizable surfaces.

II. GREEN'S FUNCTION METHODS AND SYSTEM PARAMETERS

We consider a system consisting of a 1:1 electrolyte with N_+ cations and N_- anions of diameter d confined between two polarizable surfaces placed parallel to the x-y plane and separated by a distance L in the z direction. The (periodic) box has side lengths L_x and L_y in the x and y directions. Each region has a uniform dielectric constant, which is ε_w and ε_c for the electrolyte and confining material, respectively. To investigate the ions' transport, we apply an external field **E** in the direction parallel to the confining walls. The setup is shown in Fig. 1(b).

The ion-ion electrostatic interaction that accounts for the polarization of the confining conducting surfaces is derived from the method developed in Ref. [24]. It circumvents explicit calculation of induced surface charge, applies to strong confinement ($1 < L/d < 2$), and consists of a single term for $1 < L/d \lesssim 1.5$. The method takes advantage of the short-ranged ion-ion electrostatic interaction in strong confinement by conductors, which allows us to use the minimum image convention rather than Ewald summation methods to compute the electrostatic interactions. This significantly accelerates molecular simulations, so we refer to the method as the *fast strong conducting confinement* (FSCC) method. To derive it we consider a single confined charge q_i at $\mathbf{r}_i = (0, z_i)$ on the z axis of the cylindrical coordinate system, see Fig. 1(b). The polarizable infinite planar surfaces are placed at $z = 0$ and $z = L$. The Poisson equation was solved for this setup in the context of confined ionic liquids [24]. The electrostatic potential at an arbitrary position **r**, generated by the ion q_i, is given by

$$\phi(\mathbf{r}) = \frac{4q_i}{\varepsilon_w L} \sum_{n=1}^{\infty} \sin\left(\frac{n\pi z}{L}\right) \sin\left(\frac{n\pi z_i}{L}\right) K_0\left(\frac{n\pi \Delta r}{L}\right), \quad (1)$$

where K_0 is the modified Bessel function of order 0 and $\Delta r = \sqrt{(x - x_i)^2 + (y - y_i)^2}$. For strong confinement, meaning L of order of d, just the first term ($n = 1$) of the summation in Eq. (1) is necessary because the minimal separation between two ions in the radial direction is $\Delta r_m = \sqrt{L(2d - L)}$, see Fig. 1(b). This condition implies that the argument of the modified Bessel function is at least $n\pi\sqrt{(2d/L - 1)}$, leading to a fast convergence of sum. Considering $L = 1.475d$, this gives $K_0(n\pi\sqrt{0.356}) \approx 0.13, 0.01, 0.001$, for $n = 1, 2, 3$, respectively. For the systems studied in this work, we use just the first term, $n = 1$, leading to simple expressions, derived below. For larger L, $1.5 < L/d < 2$, one needs to consider more terms in the summation, see Fig. 1(c).

The force between two ions q_i and q_j at positions $\vec{r}_i$ and $\vec{r}_j$, converting to Cartesian coordinates, is

$$F_x^{(i,j)} = \frac{4\pi q_i q_j (x_i - x_j)}{\varepsilon_w L^2 \Delta r} \sin\left(\pi \frac{z_i}{L}\right) \sin\left(\pi \frac{z_j}{L}\right) K_1\left(\pi \frac{\Delta r}{L}\right),$$

$$F_y^{(i,j)} = \frac{4\pi q_i q_j (y_i - y_j)}{\varepsilon_w L^2 \Delta r} \sin\left(\pi \frac{z_i}{L}\right) \sin\left(\pi \frac{z_j}{L}\right) K_1\left(\pi \frac{\Delta r}{L}\right),$$

$$F_z^{(i,j)} = -\frac{4\pi q_i q_j}{\varepsilon_w L^2} \cos\left(\pi \frac{z_i}{L}\right) \sin\left(\pi \frac{z_j}{L}\right) K_0\left(\pi \frac{\Delta r}{L}\right),$$

where $F_x^{(i,j)}$, $F_y^{(i,j)}$, and $F_z^{(i,j)}$ are the x, y, and z components of electrostatic force, and K_1 is the modified Bessel function of order 1.

The self-electrostatic interaction describes the interaction between an ion and the surface charge it induces. It would be computed by Eq. (1) as $r \to 0$, but K_0 diverges in this limit. In this case we consider the integral-based method [24], which gives

$$\phi_{\text{self}}(z_i) = \frac{q_i}{\varepsilon_w} \int_0^\infty \frac{2e^{-2kL} - e^{-2kz_i} - e^{2kz_i - 2kL}}{(1 - e^{-2kL})} dk.$$

The self-force acting on charge q_i in the z direction is $F_z^{\text{self}} = -\frac{q_i}{2} \frac{\partial}{\partial z_i} \phi_{\text{self}}(z_i)$, which can be written

$$F_z^{\text{self}} = \frac{q_i^2}{4L^2 \varepsilon_w} \left[\psi^{(1)}(1 - z_i/L) - \psi^{(1)}(z_i/L) \right], \qquad (2)$$

where $\psi^{(1)}$ is the polygamma function of first order.

To study ionic transport in confinement by conductors, we incorporate the FSCC method into molecular dynamics simulations. Additionally, we consider the case of confining dielectric walls using the method of periodic Green function (PGF) [25]. While both Green function methods (FSCC and PGF) agree for conducting surfaces, the FSCC method is around two orders of magnitude faster.

We investigate a 1 : 1 electrolyte under two confinement widths, $L = 1.1d$, confining the ions almost exactly to a plane, and a larger value $L = 1.475d$. The dielectric constant within the slit is $\varepsilon_w = 5\varepsilon_0$ to represent an organic solvent or strongly confined water [26]. We set $N_+ = N_- = 10$, and each ion has a charge $q_+ = e$ or $q_- = -e$ located at its center, where e is the positive elementary charge. The lateral dimensions of the simulation box are $L_x = 11.9d$ and $Ly = 12d$, which were chosen based on surface discretization that will be relevant in Sec. IV. The ions' excluded volume is represented with a truncated Lennard-Jones potential (also known as the Weeks-Chandler-Anderson potential) using an energy scale ϵ_{LJ}, with $\sigma_{\text{LJ-ion}} = d$. The walls confine the ions via a truncated Lennard-Jones potential, with $\sigma_{\text{LJ}} = 0.8353d$ and ϵ_{LJ}. The wall-ion interaction is calculated using the Lorentz-Berthelot mixing rule. The centers of the confining walls are located at $z = -0.5\sigma_{\text{LJ}}$ and $z = L + 0.5\sigma_{\text{LJ}}$. The values for the energy, mass, and distance scales are $\epsilon_{\text{LJ}} = k_B T$, where $T = 298$ K, the ion mass set to the mass of sodium $m = 22.98$ amu, and $d = 0.425$ nm, a typical size of a hydrated ion. We assume symmetry of ion mass and diameter to focus on the effect of polarization charge on ion transport. Effects due to asymmetry of other ion properties will be explored in future work. We

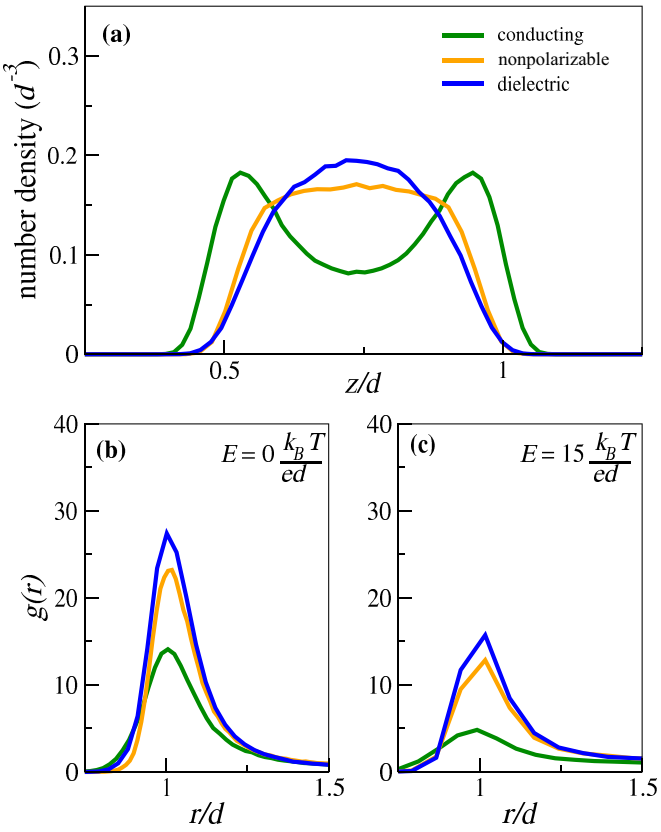

FIG. 2. Results for 1 : 1 electrolyte for various surface polarization conditions for $L = 1.475d$. (a) The ionic concentration profiles. (b) Cation-anion radial distributions with no applied electric field. (c) Cation-anion radial distributions with applied electric field $E = 15\, k_B T e^{-1} d^{-1}$.

study the ionic currents by applying an electric field $\mathbf{E} = E\hat{x}$ tangentially to the surfaces, see Fig. 1(b), and compare the results for conducting ($\varepsilon_c \to \infty$), dielectric ($\varepsilon_c = 2\varepsilon_0$), and nonpolarizable surfaces.

We perform molecular dynamics (MD) simulations using the Langevin method with a damping parameter of 100 fs and periodic boundary conditions in x and y directions. We consider 100 000 MD steps for equilibration and 100 MD steps of space between 10 000 uncorrelated samples created for further analysis.

III. EFFECTS OF CONFINEMENT AND MATERIAL POLARIZABILITY

We analyze the ionic density profiles, the current I, the radial distributions, and the conductivity of the confined ions. Figure 2(a) shows that the ions are more adsorbed to conducting surfaces and more repelled from dielectric surfaces than they are from nonpolarizable surfaces. This behavior is expected, since the ionic interactions with dielectric or conducting surfaces can be understood in terms of equally or oppositely charged images, respectively [27]. Figure 2(b) shows the pair-correlation functions between oppositely charged ions, $g(r)$, which is related to the potential of mean force between ions $w(r)$ as $g(r) = e^{-w(r)/k_B T}$. Therefore, Fig. 2(b) shows that the effective interaction between

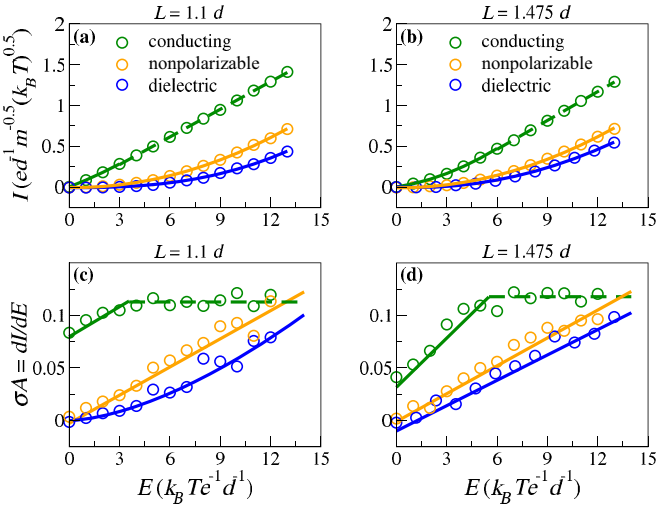

FIG. 3. Results for 1 : 1 electrolyte for various surface polarization conditions. Current as a function of applied electric field for separation (a) $L = 1.1d$ and (b) $L = 1.475d$. The electrolyte conductivity σA as a function of applied electric field for separation (c) $L = 1.1d$ and (d) $L = 1.475d$. The two regimes for conducting cases can be observed for each curve with dashed and full lines, which are fits of current curves. The current is calculated as $I = \langle \sum_{i=1}^{N_+ + N_-} q_i v_{ix}/L_x \rangle$, where q_i and v_i are the charge and the velocity of particle i.

oppositely charged ions is modified by the properties of the confining walls. The ion pairing is seen as a peak in the anion-cation radial distribution function at $r/d \approx 1$. The peak decreases by a factor of ≈ 2.5 for conducting surfaces compared to dielectric surfaces [see Fig. 2(b)], signifying that the formation of pairs is less favorable between conducting surfaces than dielectrics. The decrease in pair formation in conducting confinement occurs due to the difference in ion-ion interactions near dielectric and conducting surfaces. An ion q_i interacts with an oppositely charged ion q_j *and* with q_j's equally charged image charges near a dielectric material, *but* mostly with the q_j's opposite image charges near a conducting material. An external electric field **E** (applied in the channel's surface parallel direction) decreases the effective anion-cation attraction, but the effect due to the confining walls' polarization persists [see Fig. 2(c)].

Figures 3(a) and 3(b) show that the currents obtained with confining conductive surfaces are much higher than those obtained with dielectric surfaces. The applied electric field and the current are related as $I = A\sigma E$, where σ is the conductivity and A is the slit's cross-sectional area. A field-dependent conductivity (nonlinear I-E relationship) is essential in *memristors* [7], which are the basis of memory systems. The three I-E curves and their corresponding conductivities in Fig. 3 exhibit diverse regimes, depending on separation between surfaces and polarization. In the field range studied here, for a given value of L, the ionic current and conductivity are higher between conductors than between dielectric or nonpolarizable surfaces. At the separation distance of $L = 1.1d$ between conductors, the current is linear in almost the entire range of studied electric fields. Under such strong confinement, ions are constrained to move nearly on a plane, so the Ohmic behavior in our simulations is consistent with the two-dimensional model between conducting surfaces [19]. The ionic current between conductors at the larger separation distance ($L = 1.475d$) shows a nonlinear trend for fields below $E \sim 6\, k_B T e^{-1} d^{-1}$. For nonpolarizable and dielectric surfaces, the I-E curves present a quadratic form, which reflects the linear curves for the conductivity. The exception occurs for dielectric confinement at short separations, which data are best fitted with a $E^{2.6}$ function, which gives a $E^{1.6}$ dependence for conductivity. Combining results using conductor to nonconductor switchable materials suggests a mechanism for inducing hysteresis loops [7] in memristors.

The current nonlinear behavior can be understood in terms of the Onsager's ion-pairing theory [4,28]. According to this theory, the ions form pairs that last for a time τ_d and stay free for a time τ_a. Ion pairs have zero net charge, meaning they do not contribute to the current. Hence, a larger number of ionic pairs between dielectrics than between conductors decreases the overall current. With the increase in electric field, the ion pair's duration time τ_d decreases [reflected as a decrease of the radial distribution peak in Figs. 2(b) and 2(c)] and the current increases. Due to the weaker attraction in confinement by conductive surfaces, τ_d is shorter than between dielectric and nonpolarizable surfaces. Therefore, in confinement by conductors the ions tend to move dissociated as an electron gas (Ohmic behavior), whereas in confinement by dielectric and nonpolarizable surfaces the ion pairs persist in a broader range of electric fields. At high enough E fields all confining materials give an Ohmic response. This variety of behaviors show that the particle-particle interaction strongly influences the ionic current, revealing the modulation of surface properties to be a tool for tuning ionic behavior.

IV. EFFECTS OF THE POLARIZATION PLANE PLACEMENT

The Green function methods apply to planar confinement. For other geometries, such as conical channels suggested for current rectification [29,30], other methods are necessary. *Explicit polarization* methods incorporate the surface polarizability into ion-ion interactions by calculating the induced charge in a way that is not restricted to a specific geometry [31,32]. Conductors are implemented by imposing a uniform surface potential $\psi(\mathbf{s}) = const$. In dielectrics with no free surface charges, the electric field boundary conditions at the interface between two media are given by $\varepsilon_w \mathbf{E}_{w,n} = \varepsilon_c \mathbf{E}_{c,n}$ and $\mathbf{E}_{w,t} = \mathbf{E}_{c,t}$, where the subscripts w and c refer to the ions' solvent and confining material, respectively, and n and t indicate the perpendicular and tangential electric field components.

The electrostatic boundary conditions define the polarization plane (image plane) which represents the location of the polarization charges. In early density-functional theory studies, Lang and Kohn found that the image plane at metallic surfaces is located at the centroid of the induced charge profile [23]. Later work shows that the induced polarization charge peak resides in a range from tenths of an angstrom inside the surface nuclei to a few angstroms outside, depending on electron density of the material, external electric field, and other factors [33]. More recently, it has been suggested that

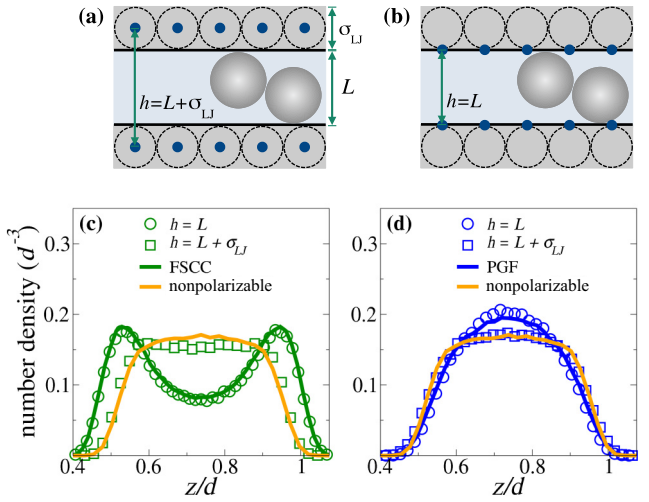

FIG. 4. Two models for charge placement, using different charge separation distances h: (a) $0.5\sigma_{LJ}$ *inside* the surfaces ($h = L + \sigma_{LJ}$) and (b) exactly on the *surface* of the material ($h = L$). Ion number density profiles for both charge placement models, compared with exact polarizable and nonpolarizable results for (c) conducting and (d) dielectric surfaces. In both figures, *inside* charge placement causes the ions to behave almost as if the surfaces were nonpolarizable.

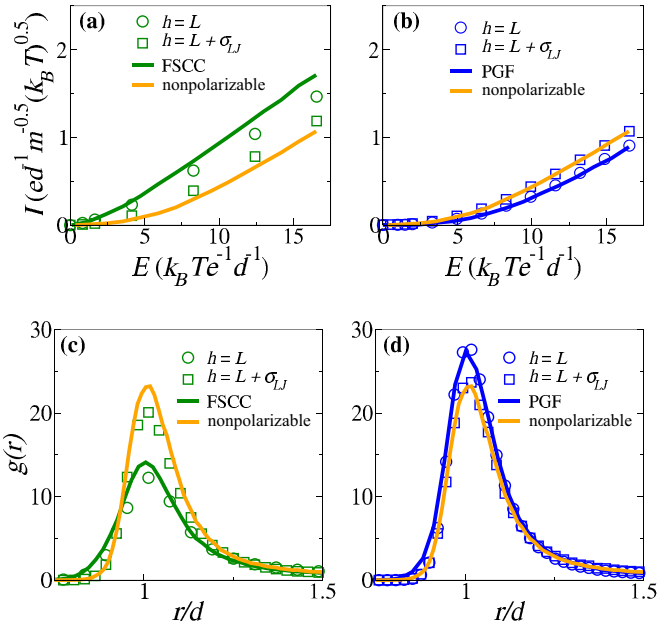

FIG. 5. Ionic current for confining (a) conducting and (b) dielectric surfaces. Cation-anion radial distribution for (c) conducting and (d) dielectric surfaces, with no applied electric field. Analogously to Fig. 4, ion current is much more significantly impacted by changing surface material for *surface* charge placement.

the image plane location affects the adsorption of charged peptide species on gold [34] and shows that the double-layer capacitance of silver and graphite surfaces depends on image plane placement [35].

In classical molecular simulations, however, the induced polarization charge is frequently placed at the center of the beads forming the surface [20,32]. For conducting surfaces, and extending the concept to dielectrics, we study the impact of this choice by placing the polarization charges (1) *inside* the channel walls [$h = L + \sigma_{LJ}$, Fig. 4(a)] or (2) on the *surface* [$h = L$, Fig. 4(b)]. Because our methods require explicit surface charge to be represented on a discrete mesh, we locate the polarization charges on a hexagonal graphene structure with an average nearest-neighbor distance of $0.332d$ on the x-y plane. All the other parameters are the same as described in Sec. II. We perform molecular dynamics simulations for only the case of $L = 1.475d$ using the polarization methods implemented in LAMMPS [36]. In conductors, a constant surface potential is maintained using the Gaussian charge model [31,37,38]. For dielectrics, the electrostatic boundary conditions are considered using a boundary element method [32]. Further details of the wall and conductor models are supplied in the Supplemental Material [39].

Figures 4(c) and 4(d) show the ion density profiles for conductive and dielectric surfaces, respectively. The figures include the profiles at the polarization charge locations of $h = L$ and $h = L + \sigma_{LJ}$. For comparison, we include the results from the Green function methods (FSCC and PGF) and for nonpolarizable systems. Placing the polarization charges on the walls' *surface* ($h = L$) leads to conductive surfaces adsorbing the ions and dielectric surfaces repelling them. For both dielectrics and conductors, the effect of surface polarization is significantly dampened when the polarization charges are located inside the surface. Placing the polarization charges *inside* the surfaces causes the profiles of polarizable systems to converge towards those of nonpolarizable systems, while placing the polarization charges on the *surface* results in profiles that overlap with the Green function methods. Similarly, the ionic current in polarizable models is close to that of nonpolarizable systems [see Figs. 5(a) and 5(b)] when the polarization plane is *inside* the surfaces. When the polarization plane is placed on the walls' *surface*s, the current is similar to that from the Green function methods. We attribute the slight discrepancy between the two methods at high fields to the discrete mesh employed in the *explicit polarization* models (see Fig. S2 in the Supplemental Material [39]). The pair-correlation functions in Figs. 5(c) and 5(d) explain the current behavior. The systems with *surface* charge placement indicate decreased ion clustering (lower peak) for conductive surfaces and enhanced ion clustering (higher peak) for dielectric materials, aligning with the Green function methods. Our findings demonstrate that both the surface polarization and the polarization plane placement modulate the ion conductance.

V. CONCLUSIONS

We study the adsorption, interactions, and current of ions confined in slitlike channels made of polarizable surfaces. The ionic current is nonlinear and shows different behavior in channels made of conductors, dielectrics, and nonpolarizable surfaces. Strong confinement and polarization effects lead to non-Ohmic ionic currents, whereas the two-dimensional transport between conductors tends to be linear. The ionic current modulation and nonlinear trend (essential for designing memristors) are caused by the screened or enhanced ionic

clustering that is different for each type of confining material. We demonstrate that location of the polarization plane and the confining distance significantly affect the confined fluid properties. Considering the surface of materials with different electronic properties is crucial for studying hybrid ionic-electronic coupling in numerous fields such as materials with neuromorphic applications, energy harvesting, and water desalination. In quantum-mechanical calculations, however, considering the coupling between ions transport and the electrons of a surface is challenging due to the differences in time and length scales. Here we employ the polarization and the polarization plane location to overcome that difficulty in a consistent way with density-functional theory.

ACKNOWLEDGMENTS

This work was supported by the National Science Foundation's MRSEC program (DMR-2308691) at the Materials Research Center of Northwestern University. A.P.d.S. thanks CNPq (303463/2021-0) and FAPERGS (19/2551-0001654-9).

A.P.d.S. and F.J.A. contributed equally to this work.

[1] J. J. Yang, D. B. Strukov, and D. R. Stewart, Memristive devices for computing, Nat. Nanotechnol. **8**, 13 (2013).

[2] Y. van de Burgt, A. Melianas, S. T. Keene, G. Malliaras, and A. Salleo, Organic electronics for neuromorphic computing, Nat. Electron. **1**, 386 (2018).

[3] P. A. Merolla, J. V. Arthur, R. Alvarez-Icaza, A. S. Cassidy, J. Sawada, F. Akopyan, B. L. Jackson, N. Imam, C. Guo, Y. Nakamura, B. Brezzo, I. Vo, S. K. Esser, R. Appuswamy, B. Taba, A. Amir, M. D. Flickner, W. P. Risk, R. Manohar, and D. S. Modha, A million spiking-neuron integrated circuit with a scalable communication network and interface, Science **345**, 668 (2014).

[4] P. Robin, N. Kavokine, and L. Bocquet, Modeling of emergent memory and voltage spiking in ionic transport through angstrom-scale slits, Science **373**, 687 (2021).

[5] T. M. Kamsma, W. Q. Boon, T. ter Rele, C. Spitoni, and R. van Roij, Iontronic neuromorphic signaling with conical microfluidic memristors, Phys. Rev. Lett. **130**, 268401 (2023).

[6] D. Kuzum, S. Yu, and H.-S. P. Wong, Synaptic electronics: Materials, devices and applications, Nanotechnology **24**, 382001 (2013).

[7] P. Robin, T. Emmerich, A. Ismail, A. Niguès, Y. You, G.-H. Nam, A. Keerthi, A. Siria, A. K. Geim, B. Radha, and L. Bocquet, Long-term memory and synapse-like dynamics in two-dimensional nanofluidic channels, Science **379**, 161 (2023).

[8] B. Cho, S. Song, Y. Ji, T.-W. Kim, and T. Lee, Organic resistive memory devices: Performance enhancement, integration, and advanced architectures, Adv. Funct. Mater. **21**, 2806 (2011).

[9] V. K. Sangwan, H.-S. Lee, H. Bergeron, I. Balla, M. E. Beck, K.-S. Chen, and M. C. Hersam, Multi-terminal memtransistors from polycrystalline monolayer molybdenum disulfide, Nature (London) **554**, 500 (2018).

[10] F. Gärisch, G. Ligorio, P. Klein, M. Forster, U. Scherf, and E. J. W. List-Kratochvil, Organic synaptic diodes based on polymeric mixed ionic-electronic conductors, Adv. Electron. Mater. **8**, 2100866 (2022).

[11] R. Wu, M. Matta, B. D. Paulsen, and J. Rivnay, Operando characterization of organic mixed ionic/electronic conducting materials, Chem. Rev. **122**, 4493 (2022).

[12] I. Riess, Mixed ionic–electronic conductors—Material properties and applications, Solid State Ionics **157**, 1 (2003), Proceedings of the 6th International Symposium on Systems with Fast Ionic Transport (ISSFIT).

[13] J. Rivnay, S. Inal, B. A. Collins, M. Sessolo, E. Stavrinidou, X. Strakosas, C. Tassone, D. M. Delongchamp, and G. G. Malliaras, Structural control of mixed ionic and electronic transport in conducting polymers, Nat. Commun. **7**, 11287 (2016).

[14] I. S. Kim, V. K. Sangwan, D. Jariwala, J. D. Wood, S. Park, K.-S. Chen, F. Shi, F. Ruiz-Zepeda, A. Ponce, M. Jose-Yacaman, V. P. Dravid, T. J. Marks, M. C. Hersam, and L. J. Lauhon, Influence of stoichiometry on the optical and electrical properties of chemical vapor deposition derived MoS2, ACS Nano **8**, 10551 (2014).

[15] H. Qiu, T. Xu, Z. Wang, W. Ren, H. Nan, Z. Ni, Q. Chen, S. Yuan, F. Miao, F. Song, G. Long, Y. Shi, L. Sun, J. Wang, and X. Wang, Hopping transport through defect-induced localized states in molybdenum disulphide, Nat. Commun. **4**, 2642 (2013).

[16] Y. Wang, T. Seki, X. Liu, X. Yu, C.-C. Yu, K. F. Domke, J. Hunger, M. T. M. Koper, Y. Chen, Y. Nagata, and M. Bonn, Direct probe of electrochemical pseudocapacitive pH jump at a graphene electrode, Angew. Chem., Int. Ed. **62**, e202216604 (2023).

[17] D. T. Limmer, C. Merlet, M. Salanne, D. Chandler, P. A. Madden, R. van Roij, and B. Rotenberg, Charge fluctuations in nanoscale capacitors, Phys. Rev. Lett. **111**, 106102 (2013).

[18] A. Schlaich, D. Jin, L. Bocquet, and B. Coasne, Electronic screening using a virtual Thomas–Fermi fluid for predicting wetting and phase transitions of ionic liquids at metal surfaces, Nat. Mater. **21**, 237 (2022).

[19] N. Kavokine, P. Robin, and L. Bocquet, Interaction confinement and electronic screening in two-dimensional nanofluidic channels, J. Chem. Phys. **157**, 114703 (2022).

[20] F. Jiménez-Ángeles, A. Ehlen, and M. Olvera de la Cruz, Surface polarization enhances ionic transport and correlations in electrolyte solutions nanoconfined by conductors, Faraday Discuss. **246**, 576 (2023).

[21] E. H. Lieb and B. Simon, Thomas-Fermi theory revisited, Phys. Rev. Lett. **31**, 681 (1973).

[22] C. Y. Son and Z.-G. Wang, Image-charge effects on ion adsorption near aqueous interfaces, Proc. Natl. Acad. Sci. USA **118**, e2020615118 (2021).

[23] N. D. Lang and W. Kohn, Theory of metal surfaces: Induced surface charge and image potential, Phys. Rev. B **7**, 3541 (1973).

[24] M. Girotto, A. P. dos Santos, and Y. Levin, Simulations of ionic liquids confined by metal electrodes using periodic Green functions, J. Chem. Phys. **147**, 074109 (2017).

[25] A. P. dos Santos, M. Girotto, and Y. Levin, Simulations of Coulomb systems confined by polarizable surfaces using periodic Green functions, J. Chem. Phys. **147**, 184105 (2017).

[26] L. Fumagalli, A. Esfandiar, R. Fabregas, S. Hu, P. Ares, A. Janardanan, Q. Yang, B. Radha, T. Taniguchi, K. Watanabe, G. Gomila, K. S. Novoselov, and A. K. Geim, Anomalously low dielectric constant of confined water, Science **360**, 1339 (2018).

[27] J. Jackson, *Classical Electrodynamics* (Wiley, New York, 1998)

[28] L. Onsager, Deviations from Ohm's law in weak electrolytes, J. Chem. Phys. **2**, 599 (1934).

[29] J. Gao, A. R. Koltonow, K. Raidongia, B. Beckerman, N. Boon, E. Luijten, M. Olvera de la Cruz, and J. Huang, Kirigami nanofluidics, Mater. Chem. Front. **2**, 475 (2018).

[30] W. Q. Boon, T. E. Veenstra, M. Dijkstra, and R. van Roij, Pressure-sensitive ion conduction in a conical channel: Optimal pressure and geometry, Phys. Fluids **34**, 101701 (2022).

[31] L. J. V. Ahrens-Iwers, M. Janssen, S. R. Tee, and R. H. Meißner, Electrode: An electrochemistry package for atomistic simulations, J. Chem. Phys. **157**, 084801 (2022).

[32] T. D. Nguyen, H. Li, D. Bagchi, F. J. Solis, and M. Olvera de la Cruz, Incorporating surface polarization effects into large-scale coarse-grained molecular dynamics simulation, Comput. Phys. Commun. **241**, 80 (2019).

[33] N. B. Luque and W. Schmickler, The electric double layer on graphite, Electrochim. Acta **71**, 82 (2012).

[34] H. Heinz, K. C. Jha, J. Luettmer-Strathmann, B. L. Farmer, and R. R. Naik, Polarization at metal–biomolecular interfaces in solution, J. R. Soc., Interface **8**, 220 (2011).

[35] W. Schmickler, The electronic response of the metal in simulations of the electric double layer, J. Electroanal. Chem. **856**, 113664 (2020).

[36] A. P. Thompson, H. M. Aktulga, R. Berger, D. S. Bolintineanu, W. M. Brown, P. S. Crozier, P. J. in 't Veld, A. Kohlmeyer, S. G. Moore, T. D. Nguyen, R. Shan, M. J. Stevens, J. Tranchida, C. Trott, and S. J. Plimpton, LAMMPS – A flexible simulation tool for particle-based materials modeling at the atomic, meso, and continuum scales, Comput. Phys. Commun. **271**, 108171 (2022).

[37] J. I. Siepmann and M. Sprik, Influence of surface topology and electrostatic potential on water/electrode systems, J. Chem. Phys. **102**, 511 (1995).

[38] S. K. Reed, O. J. Lanning, and P. A. Madden, Electrochemical interface between an ionic liquid and a model metallic electrode, J. Chem. Phys. **126**, 084704 (2007).

[39] See Supplemental Material at http://link.aps.org/supplemental/10.1103/PhysRevResearch.5.043174 for details regarding choice of wall softness, Gaussian charge conductor model, and polarization charge surface meshing parameters.